Numerical analysis of flow pattern map of R600a in a collector/evaporator of a solar-assisted heat pump

Análisis numérico de los mapas de patrones de flujo del refrigerante R600a en un colector/evaporador de una bomba de calor asistida por energía solar

William Quitiaquez[1],* iD, Eduardo Cortez[2] iD, Karen Anchapaxi[2] iD,

C.A. Isaza-Roldán[3] iD, César Nieto-Londoño[4] iD, Patricio Quitiaquez[1] iD,

Fernando Toapanta-Ramos[1] iD

Abstract

This research work presents a detailed description of the flow patterns maps generated in a horizontal pipe of the collector/evaporator of a direct-expansion solar-assisted heat pump, using R600a refrigerant as working fluid. The study was performed in a pipe with an internal diameter of 3.8 mm and a length of 1000 mm, mass velocities varying between 197.59 and 267.26 kg·m^{-2}·s^{-1} and heat flux between 72.83 and 488.27 W·m^{-2}; during the experimental tests, an incident solar radiation between 0 and 652.9 W·m^{-2} was present. The Wojtan, Ursenbacher and Thome correlation was considered for the analysis and the model used does not require iterative calculations; moreover, it carries out a detailed analysis of the different zones present along the pipe. The predominant zones in this study are intermittent, annular and dryout, found in the five tests, however, due to the working conditions in all tests with the exception of test A, mist and stratified-wavy flow were found.

Keywords: Flow patterns, two-phase flow, heat transfer, R600a

Resumen

En la presente investigación se detallan los mapas de patrones de flujo que se generan en una tubería horizontal de un colector/evaporador componente de una bomba de calor de expansión directa asistida por energía solar, utilizando el refrigerante R600a como fluido de trabajo. El estudio se realizó en una tubería de 3,8 mm de diámetro interno y 1000 mm de longitud, las velocidades de masa variaron entre 197,59 y 267,26 kg·m^{-2}·s^{-1}, el flujo de calor entre 72,83 y 488,27 W·m^{-2}, durante las pruebas experimentales se presentó una radiación solar incidente entre 0 y 652,9 W·m^{-2}. Se consideró para el análisis la correlación de Wojtan, Ursenbacher y Thome, el modelo utilizado no requiere de cálculos iterativos, además, plantea un análisis detallado de las diferentes zonas presentes a lo largo de la tubería, evidenciando una mayor precisión en los resultados. Las zonas predominantes en los resultados de este estudio son: intermitente, anular y secado, encontrados en las cinco pruebas, sin embargo, por las condiciones de trabajo en todas las pruebas a excepción de la prueba A, se encontró el flujo niebla y estratificado-ondulado.

Palabras clave: patrones de flujo, flujo bifásico, transferencia de calor, R600a

[1],*Carrera de Ingeniería Mecánica - Programa de Maestría en Producción y Operaciones Industriales / GIERIMP, Universidad Politécnica Salesiana, Quito, Ecuador. Corresponding author ✉: wquitiaquez@ups.edu.ec.

[2]Carrera de Ingeniería Mecánica, Universidad Politécnica Salesiana, Quito, Ecuador.

[3]Centro de Investigación en Refrigeración y Aire Acondicionado, Universidad Pontificia Bolivariana, Colombia.

[4]Facultad de Ingeniería Aeroespacial, Universidad Pontificia Bolivariana, Colombia.

1. Introduction

From past decades until now different protocols have been implemented to help mitigate environmental problems [1, 2]. Abas *et al.* [3] indicate that refrigeration systems are under a prescribed permission period of the Kyoto Protocol which, together with the European Union and the Paris Agreement, emphasize on the elimination of refrigerants that harm the ozone layer and proposes to replace them by natural refrigerants. For this purpose, research studies are conducted across the globe using hydrocarbon refrigerants, such as R290 and R600a, which show an ozone depletion potential (ODP) of 0 and a global warming potential (GWP) of 3 [4].

Yu *et al.* [5] use the R290 and R600a refrigerants as an alternative to R134a. Results indicate that refrigeration systems consume less electricity and the refrigerant load is 30 to 60 % smaller compared to the load of the R134a, concluding that it improves the energy factor of refrigeration systems reducing the refrigerant load with the R600a and decreasing even more the direct emissions to the environment produced by refrigerants [6].

The flow patterns predict the hydrodynamics of the flow and the heat transfer between a pipe and the fluid that it transports; due to its larger heat transfer rate, the refrigerant will rapidly change phase and enter the compressor in pure vapor phase [7]. The flow regime that predicts an almost total phase change is the mist flow pattern visualized at the outlet of the collector/evaporator, which is present in research works such as the one conducted by Wojtan *et al.* [8].

The Wojtan *et al.* correlation [8] is analyzed to determine the flow patterns that may appear in horizontal pipes, since they propose various modifications to the map proposed by Kattan *et al.* [9]. The correlation by Wojtan *et al.* [8] does not involve iterative calculations and indicates that the stratified-wavy zone is further subdivided in three zones, namely slug, slug + stratified-wavy and stratified-wavy; in addition, it is mentioned an extra analysis in the transition of the zones from annular to dryout and from dryout to mist, and likewise it is known the beginning and the end of the dryout zone that may appear in this type of pipes.

Mashouf *et al.* [10] conducted a research working with horizontal tubes and R600a refrigerant; they showed different flow patterns at mass velocities between 114 and 368 kg·m^{-2}·s^{-1}, with saturation temperature between 38 and 42 °C and quality of 0.8 for the boiling process of the refrigerant. The results obtained were an intermittent and annular flow in a dimpled tube, whereas for a smooth tube it was observed an intermittent, annular and stratified-wavy flow. Similarly, Vahabi *et al.* [11] conducted a study of the flow patterns in a copper tube with an internal diameter of 8.7 mm and a length of 1200 mm, using

R600a refrigerant. The test was carried out with mass velocities (GA) between 155 and 470 kg·m^{-2}·s^{-1} and quality between 0.05 and 0.78, finding the flows intermittent, annular and stratified-wavy for the smooth tube.

De Oliveira *et al.* [12] determined the pressure drop and the flow patterns when using R600a refrigerant, in a horizontal tube with an internal diameter of 1 mm. The heat flux conditions fluctuated between 5 and 60 kW·m^{-2}, mass velocities between 240 and 480 kg·m^{-2}·s^{-1} and a saturation temperature of 25 °C during the boiling process; they were able to determine that the predominant flows are plug, slug and annular.

Yang *et al.* [13] studied the two-phase flow patterns that may appear in a horizontal pipe with an internal diameter of 6 mm, using the R600a refrigerant. The values obtained experimentally were: heat fluxes (q) between 10.6 and 75 kW·m^{-2}, mass velocities between 67 and 194 kg·m^{-2}·s^{-1} and saturation pressures between 0.215 and 0.415 MPa. Using a high-speed camera, they observed plug, stratified-wavy, slug and annular flows.

Zhu *et al.* [14] investigated the flow patterns during the boiling process of R32 refrigerant in horizontal mini channels, working with internal diameters of 1 and 2 mm, saturation temperatures between 10 and 20 °C, mass velocities between 500 and 600 kg·m^{-2}·s^{-1}, heat fluxes between 10 and 30 ·m^{-2} and vapor qualities between 0 and 1. The flows observed were slug, annular, dryout, mist and stratified. They determined that the slug flow region is small when the mass velocity increases and is larger when the tube diameter, the saturation temperature or the heat flux increase. For the annular region, it is smaller when the tube diameter, the saturation temperature, the heat flux or the mass velocity increase. The mist flow region has a larger presence when the saturation temperature, the mass velocity or the heat flux increase, and it is reduced when the tube diameter increases.

Zhuang *et al.* [15] observed the flows: plug, slug, intermittent and annular, where they concluded that vapor qualities decrease as the mass velocity increase, whereas the variation of the saturation pressure does not have larger influence in the zones that may be present in the analyses. In their research work about flow patterns, Liu *et al.* [16] identified six zones where the stratified flow only exists when the mass velocity is low, whereas, for the transition from intermittent to annular flow, it will depend on the mass velocity and on the heat flux, i.e., if they increase the transition line will change to a lower quality.

De Oliveira *et al.* [17] studied the boiling heat transfer using R600a refrigerant as working fluid in a horizontal pipe with an internal diameter of 1 mm. The tests were conducted using ranges of heat flux and mass velocity from 5 to 60 kW·m^{-2} and from 240 to 480 kg·m^{-2}·s^{-1}, respectively, and also a saturation temperature of 25 ºC. The flow patterns observed

Quitiaquez et al. / Numerical analysis of flow pattern map of R600a in a collector/evaporator of a solar-assisted heat pump

113

in the tests conducted were annular-wavy, annular smooth, slug and plug, with the annular flows being the predominant ones in all experimental tests.

Nasr *et al.* [18] investigated the heat transfer during the boiling of R600a in a horizontal tube with an internal diameter of 8.7 mm. The tests were conducted varying the ranges of mass velocity and heat flux from 130 to 380 kg·m^{-2}·s^{-1} and from 10 to 27 kW·m^{-2}, respectively. For quality values up to 0.7 the predominant flow patterns in all experimental tests were intermittent and annular.

The present study was conducted to investigate the flow pattern maps in a collector/evaporator on which there is incident solar radiation, using R600a refrigerant as working fluid during the boiling process. For this purpose, five experimental tests were carried out at different times, where the flow transition will be determined based on the correlation proposed by Wojtan *et al.* [8].

2. Materials and methods

The combination of a heat pump and solar energy is known as solar-assisted heat pump (SAHP) system. When collector and evaporator are merged in a single component, the system becomes a direct expansion solar-assisted heat pump (DX-SAHP) [19]. The coefficient of operation (COP) of DX-SAHP systems is above the one corresponding to conventional heat pump systems, due to the high temperatures generated by its solar energy source [20]. The DX-SAHP systems have a great potential in different applications, such as heating rooms and water, and are constituted by a collector/evaporator, a compressor, a condenser and an expansion valve [21].

The working cycle starts when the refrigerant at low temperature and pressure enters the collector/evaporator from the expansion valve, and then vaporizes when receiving the incident solar radiation. Upon arrival to the compressor the fluid is compressed increasing its temperature and pressure, and subsequently the vapor flows to the condenser and releases heat to its container [22]. Afterwards, the expansion valve reduces the temperature and pressure of the refrigerant coming

from the condenser, and finally the refrigerant enters the collector/evaporator and the process is repeated. Figure 1 shows a scheme of the DX-SAHP system constructed [23].
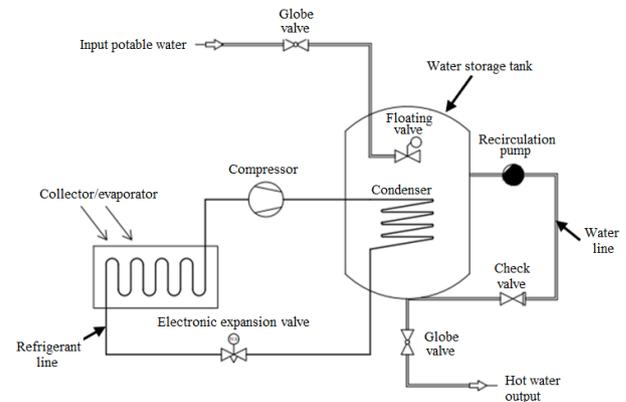

Figure 1. Proposed DX-SAHP system

2.1. Collector/evaporator

Figure 2 shows a scheme of the collector/evaporator used for analyzing the flow pattern maps, from which the experimental data for the analysis were obtained. The dimensions of the horizontal pipe used inside the collector/evaporator are: inner diameter 3.8 mm, pipe length 1000 m, collector width 223.4 mm and collector cross-sectional area 223400 mm^2.
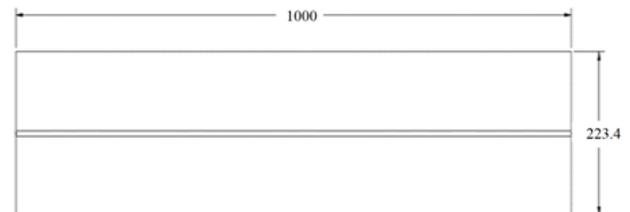

Figure 2. Schematic diagram of the collector/evaporator [2]

Operating tests were conducted at different times; Table 1 presents the most relevant experimental data.

Table 1. Experimental data for 5 different tests

Variables	Test A	Test B	Test C	Test D	Test E
Time	12:15	12:40	12:30	16:45	20:40
Ambiente temperature [°C]	17,6	18,3	17,9	15,4	12
Average incident solar radiation [W·m^{-2}]	464,1	652,9	582,6	123,22	0
Mass Flow [kg·s^{-1}]	0,00268	0,00303	0,00295	0,0026	0,00224
Vapor quality[-]	0,176	0,256	0,215	0,2305	0,2325
Superface temperature [°C]	14,5	14,5	14,5	12,6	9,5

2.2. Correlation by Wojtan, Ursenbacher and Thome

The equations for determining each of the zones that may be present in the collector/evaporator, are identified from the study conducted by Wojtan et al. [8], which is an update of the Kattan et al. [9] correlation. The advantage of using this correlation is that it involves no iterative calculation, being its study reliable and one of the most up-to-date and implemented in several research works, such as the ones conducted by Singh et al. [24] and Yang and Hrnjak [25].

2.2.1. Void fraction and stratified flow

Wojtan et al. [8] propose equation (1) as the way to obtain the void fraction, whereas the stratified angle is obtained from equation (2), moreover, it is necessary to know the height of liquid and the nondimensional perimeter of the interface, shown in equations (3) and (4), respectively [26].

$$\alpha = \frac{x}{\rho_v}\left\{ \begin{array}{l} [1+0.12(1-x)]\left(\frac{x}{\rho_v}+\frac{1-x}{\rho_L}\right)\dots \\ \dots + \frac{1.18(1-x)[g\sigma(\rho_L-\rho_v)]^{0.25}}{G_A\rho_L^{0.5}} \end{array} \right\}^{-1} \quad (1)$$

$$\theta_{strat} = 2\pi - 2\left\{ \begin{array}{l} \pi(1-\alpha)+\left(\frac{3\pi}{2}\right)^{\frac{1}{3}}\dots \\ \dots\left[1-2(1-\alpha)+(1-\alpha)^{\frac{1}{3}}-\alpha^{\frac{1}{3}}\right]\dots \\ \dots-\frac{1}{200}(1-\alpha)\alpha[1-2(1-\alpha)]\dots \\ \dots\left[1+4\left[(1-\alpha)^2+\alpha^2\right]\right] \end{array} \right\} \quad (2)$$

$$h_{Ld} = 0.5\left[1-cos\left(\frac{2\pi-\theta_{strat}}{2}\right)\right] \quad (3)$$

$$P_{id} = sin\left(\frac{2\pi-\theta_{strat}}{2}\right) \quad (4)$$

2.2.2. Stratified to stratified-wavy flow

Wojtan et al. [8] propose equation (5) as the calculation required to obtain the stratified flow, where $G_{strat} = G_{strat}(x_{IA})$ a $(x < x_{IA})$ and indicates that the flow is stratified when $G_A < G_{strat}$.

$$G_{strat} = \left[\frac{(226.3)^2 A_{Ld}A_{vd}^2\rho_v(\rho_L-\rho_v)g\mu_L}{x^2(1-x)\pi^3}\right]^{\frac{1}{3}} \quad (5)$$

2.2.3. Limit between stratified-wavy to intermittent annular flow

Equation 6 indicates the analysis necessary for the calculation in the wavy zone, indicating that three different zones may be found, namely:

Slug zone: $G > G_{wavy}(x_{IA})$

Slug/stratified-wavy zone:
$G_{strat} < G_A < G_{wavy}(x_{IA}$ and $x < x_{IA}$
Stratified-wavy zone: $x \geq x_{IA}$

$$G_{wavy} = \left\{ \begin{array}{l} \frac{16A_{vd}^3 gD\rho_L\rho_v}{x^2\pi^2[1-(2h_{Ld}-1)^2]^{0.5}}\dots \\ \dots\left[\frac{\pi^2}{25h_{Ld}^2}\left(\frac{We}{Fr}\right)_L^{-1}+1\right] \end{array} \right\}^{0.5} + 50 \quad (6)$$

2.2.4. Transition from intermittent to annular

Wojtan et al. [8], Yang et al. [27], indicate that equation (7) is necessary to determine the transition from intermittent to annular flow.

$$x_{IA} = \left\{ \left[0.34^{\frac{1}{0.875}}\left(\frac{\rho_v}{\rho_L}\right)^{-\frac{1}{1.75}}\left(\frac{\mu_v}{\mu_L}\right)^{\frac{1}{7}}\right]+1 \right\}^{-1} \quad (7)$$

2.2.5. Annular to dryout

Equation (8) shows the analysis that should be considered when determining the dryout zone, proposed by Wojtan et al. [8] and used by Yang et al. [27].

$$G_{dryout} = \left\{ \begin{array}{l} \frac{1}{0.235}\left[ln\left(\frac{0.58}{x}\right)+0.52\right]\left(\frac{D}{\rho_v\sigma}\right)^{-0.17}\dots \\ \dots\left[\frac{1}{gD\rho_v(\rho_L-\rho_v)}\right]^{-0.37}\dots \\ \dots\left(\frac{\rho_v}{\rho_L}\right)^{-0.25}\left(\frac{\dot{q}}{\dot{q}_{crit}}\right)^{-0.70} \end{array} \right\}^{0.926} \quad (8)$$

2.2.6. Dryout to mist

The calculation for the change from dryout to mist flow is determined from the equation (9) proposed by Wojtan et al. [8].

$$G_{mist} = \left\{ \begin{array}{l} \frac{1}{0.0058}\left[ln\left(\frac{0.61}{x}\right)+0.57\right]\left(\frac{D}{\rho_v\sigma}\right)^{-0.38}\dots \\ \dots\left[\frac{1}{gD\rho_v(\rho_L-\rho_v)}\right]^{-0.15}\dots \\ \dots\left(\frac{\rho_v}{\rho_L}\right)^{0.09}\left(\frac{\dot{q}}{\dot{q}_{crit}}\right)^{-0.27} \end{array} \right\}^{0.926} \quad (9)$$

In order to define the transitions in the quality range it is necessary to know the following conditions [8]:

If: $G_{strat} \geq G_{dryout} \Rightarrow G_{dryout} = G_{strat}$
If: $G_{wavy} \geq G_{dryout} \Rightarrow G_{dryout} = G_{wavy}$

However, for the dryout and mist equations, the maximum value of quality is 0.99 specified by Wojtan et al. [8]- [28] and De Oliveira et al. [12]- [29].

Quitiaquez et al. / Numerical analysis of flow pattern map of R600a in a collector/evaporator of a solar-assisted heat pump

115

3. Results and discussion

The flow pattern maps corresponding to each of the tests conducted at different times are obtained from experimental data and the correlation proposed by Wojtan *et al.* [8].

Each of the zones present in the flow pattern maps are identified according to the following nomenclature: Intermittent (I), Annular (A), Stratified (S), Stratified-wavy (SW), Dryout (D) and Mist (M). As the refrigerant circulates along the pipe of the collector/evaporator its quality increases, giving rise to the presence of the different flow patterns.

3.1. Flow pattern maps in different experimental tests

3.1.1. Flow pattern map for test A

Figure 3 shows the flow pattern map obtained at 12:15.

The mass velocity of 236.5 $kg \cdot m^{-2} \cdot s^{-1}$ indicates that the zones present in this pipe of the collector/evaporator are intermittent, annular and dryout, with quality ranges 0.176-0.2686, 0.2686-0.9484 and 0.9484-0.99, respectively. It is shown the largest visualization range in the annular zone, whereas the dryout zone is the one with the smallest visualization.
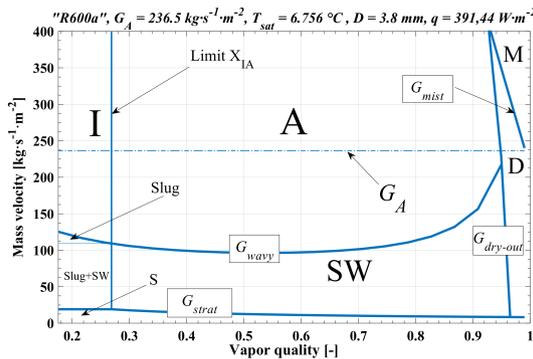
Figure 3. Flow pattern map for test A for the R600a refrigerant with T_{sat} = 6,756 °C, D = 3,8 mm, q = 391,44 $W \cdot m^{-2}$ and G_A = 236,5 $kg \cdot m^{-2} \cdot s^{-1}$

3.1.2. Flow pattern map for test B

Test B was conducted at 12:40, obtaining intermittent, annular, dryout and mist flow patterns, which are visualized in Figure 4. Compared to test A, a new zone appears with a mass velocity of 267.26 $kg \cdot m^{-2} \cdot s^{-1}$ and quality ranges 0.256-0.283, 0.283-0.941, 0.98-0.979 and 0.979-0.99, respectively, for the four zones present.

The zone with largest visualization is the annular, due to the extended quality range, whereas the intermittent zone is the one that shows the smallest visualization due to its reduced quality range.
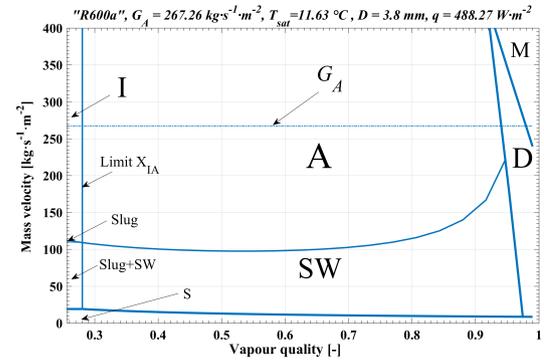
Figure 4. Flow pattern map for test B for the R600a refrigerant with T_{sat} = 11,63 °C, D = 3,8 mm, q = 488,27 $W \cdot m^{-2}$ and G_A = 267,26 $kg \cdot m^{-2} \cdot s^{-1}$

3.1.3. Flow pattern map for test C

Figure 5 shows the flow patterns for test C from the data obtained at 12:30, with a mass velocity of 260.115 $kg \cdot m^{-2} \cdot s^{-1}$. Four zones are present, namely: intermittent, annular, dryout and mist, located at the quality ranges 0.215-0.275, 0.275-0.943, 0.943-0.982 and 0.982-0.99, respectively.

In both tests A and B, the zone with largest visualization is the annular, and a small range is shown by the intermittent flow and the dryout zone.
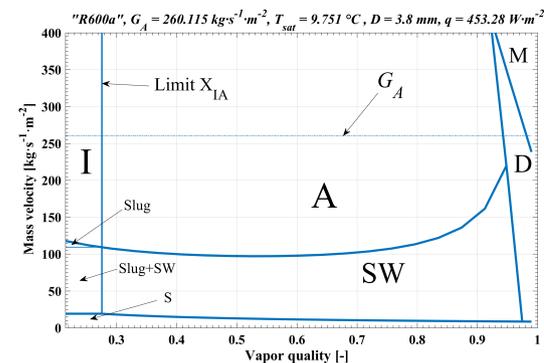
Figure 5. Flow pattern map for test B for the R600a refrigerant with T_{sat} = 9,751 °C, D = 3,8 mm, q = 453,28 $W \cdot m^{-2}$ and G_A = 260,115 $kg \cdot m^{-2} \cdot s^{-1}$

3.1.4. Flow pattern map for test D

The flow pattern map obtained from the experimental data taken at 16:45 with a mass velocity of 229.43 $kg \cdot m^{-2} \cdot s^{-1}$, shows the zones: intermittent, annular, stratified-wavy and dryout, as indicated in Figure 6.

The quality ranges present according to the flows are 0.231-0.267, 0.267-0.952, 0.952-0.961 and 0.961-0.99, respectively. The zone with the largest visualization is the annular, due to its quality range, whereas the remaining zones are present in smaller quality ranges. The operating conditions are different, and

both the mass velocity and the time for taking the data have influence, which results in the presence of a new zone, the stratified-wavy.
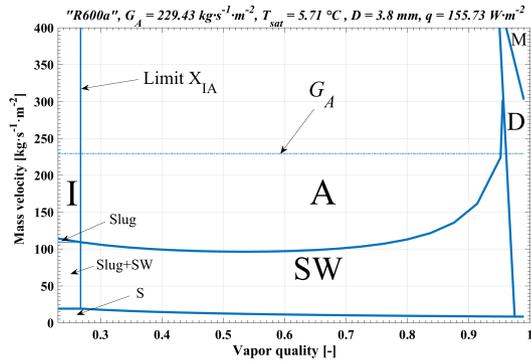

Figure 6. Flow pattern map for test B for the R600a refrigerant with T_{sat} = 5,71 °C, D = 3,8 mm, q = 155,73 W·m^{-2} and G_A = 229,43 kg·m^{-2}·s^{-1}

3.1.5. Flow pattern map for test E

Figure 7 indicates the flow pattern map for test E, obtained from the experimental data taken at 20:40 with a mass velocity of 197.59 kg·m^{-2}·s^{-1}, where the flow patterns that appear in this test are intermittent, annular, stratified wavy and dryout.

The range with the largest visualization is the one corresponding to the annular zone, whereas the intermittent and dryout zones are smaller. As it was the case for test D, the stratified-wavy zone appears because the mass velocity is smaller than in previous cases.
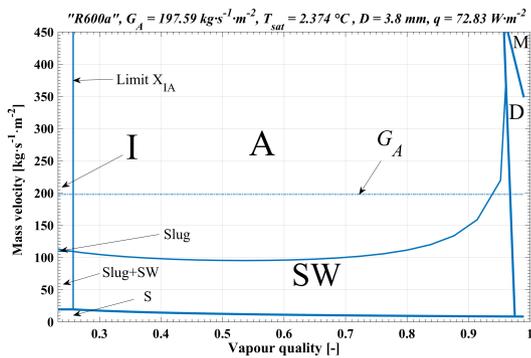

Figure 7. Flow pattern map for test B for the R600a refrigerant with T_{sat} = 2,374 °C, D = 3,8 mm, q = 72,83 W·m^{-2} and G_A = 197,59 kg·m^{-2}·s^{-1}

All tests indicate that flow patterns vary depending on the operating conditions, and thus it is determined that for a larger mass velocity the mist flow tends to be present, while if it decreases the stratified-wavy zone may appear. In addition, of the zones present in the five tests, the one with the best visualization and a larger quality range is the annular flow, which is the

predominant one in this study, as well as the intermittent and dryout zones, but with a smaller quality range.

3.2. Comparison of the flow patterns at different times

Hereafter, an analysis is conducted based on times and on the results obtained regarding the flow patterns, as well as the difference in their operating conditions.

3.2.1. Comparison between test A and test B

Figure 8 shows a comparison of the results between test A carried out at 12:15 and test B at 12:40. The incident solar radiations were 464.1 and 652.9 W·m^{-2}, respectively, and the mass velocities were 236.5 and 267.26 kg·m^{-2}·s^{-1}, respectively. It may be observed that the limits between the annular flow and the stratified-wavy and mist flows do not vary, whereas there is a small mismatch in the limit of the dryout zone, as well as the intermittent-annular limit, in which the initial qualities vary from 0.176 to 0.256.
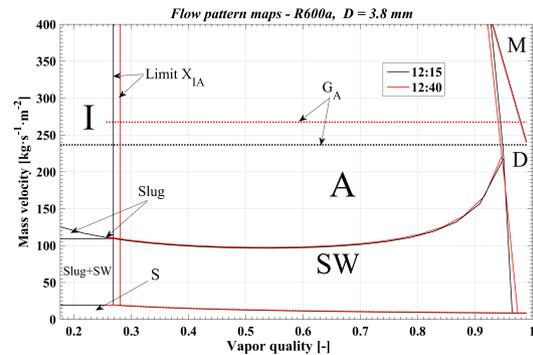

Figure 8. Comparison of the maps corresponding to tests A and B at 12:15 and 12:40, respectively

3.2.2. Comparison between test A and test D

Figure 9 shows a comparison between tests A and D, with data taken at 12:15 and 16:45, with incident solar radiations of 391.44 and 155.73 W·m^{-2}, respectively, and mass velocities of 236.5 and 229.43 kg·m^{-2}·s^{-1}, respectively. The limits between stratified and wavy do not vary, which is not the case for the remaining limits.

In case of test B, the mass velocity does not indicate that the stratified-wavy flow appears in this test, however, in test D the mass velocity is smaller and the stratified-wavy zone is present. On the other hand, the limits of the dryout and mist zones move to the right due to the increment of the incident solar radiation.
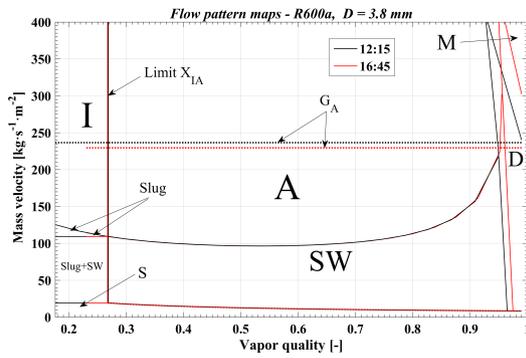
Quitiaquez et al. / Numerical analysis of flow pattern map of R600a in a collector/evaporator of a solar-assisted heat pump

117

Figure 9. Comparison of the maps corresponding to tests A and D at 12:15 and 16:45, respectively

3.2.3. Comparison between test D and test E

Figure 10 shows a comparison between tests D and E, with experimental data taken at 16:45 and 20:40, incident solar radiations of 123.22 and 0 W·m^{-2} and mass velocities of 229.43 and 197.59 kg·m^{-2}·s^{-1}, respectively. The limits of the stratified-wavy line show no variation, whereas the limits of the dryout and mist zones show a trend to the right when the incident solar radiation decreases at high quality values. Both tests indicate the presence of the stratified-wavy zone with the aforementioned values of mass velocity, however, for test D there is a better visualization of the flow because the mass velocity decreases due to the incident solar radiation of 0 W·m^{-2}.
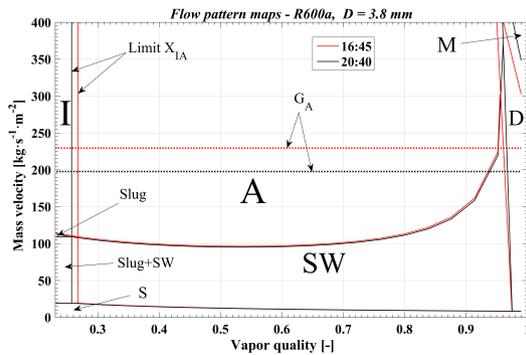

Figure 10. Comparison of the maps corresponding to tests D and E at 16:45 and 20:40, respectively

3.2.4. Comparison between test A and test E

Figure 11 displays a comparison of the flow pattern maps between tests A and E, with working hours of 12:15 and 20:40, incident solar radiations of 464.1 and 0 W·m^{-2} and mass velocities of 236.5 and 197.59 kg·m^{-2}·s^{-1}, respectively. The stratified-wavy limit shows no variation, whereas the dryout and mist limits move to the right compared to the resulting limits at noon. The difference between tests A and E for the

aforementioned velocities indicate that the stratified-wavy flow appears only in test E, not in test A.

3.2.5. Comparison of tests A, D and E

Figure 12 shows a comparison between tests A, D and E with working hours 12:15, 16:45 and 20:40, and incident solar radiations of 464.1, 123.22 and 0 W·m^{-2}, respectively. It is analyzed that the mass velocity in the plot is directly proportional to the solar radiation.
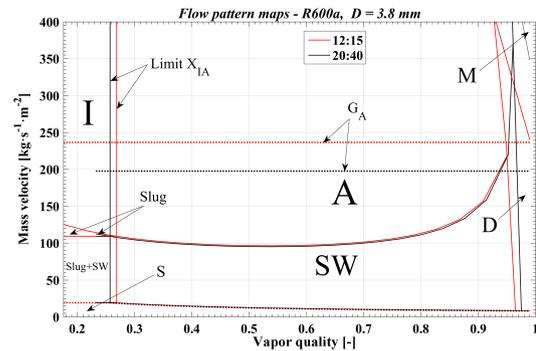

Figure 11. Comparison of the maps corresponding to tests A and E

When reducing both variables, the dryout and mist zones extend to the right with high quality values, whereas the stratified-wavy limits show no variation. It is indicated how the x_{IA} limit varies at the initial qualities. Zones that are present in the pipe according to each condition may be identified based on the mass velocity, if it is higher it will correspond to test A and if it is lower it corresponds to tests D and E. The zones present in test A are intermittent, annular and dryout, whereas for tests D and E the zones present are intermittent, annular, stratified-wavy and dryout.
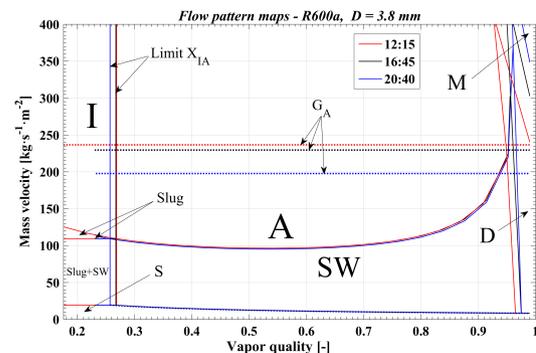

Figure 12. Comparison of the flow pattern maps with incident solar radiation at different times

In the different maps obtained, test A shows the best results due to its lower initial quality, the limits within the plot observed in Figure 3 are similar to the model by Wojtan *et al.* [8] considered for the analysis of the boiling fluid. In addition, one of the

predominant conditions in a DX-SAHP system is to have a working fluid in vapor phase at the outlet of the collector/evaporator; the flow patterns that meet this condition are dryout and mist, which are present in the larger quality range 0.941-0.99 for test B observed in Figure 4.

It is evidenced in Figure 13 the relationship between flow patterns and heat transfer coefficient (HTC); the flow patterns base their importance indicating the phase change of a refrigerant that flows within a pipe. This figure shows the intermittent, annular, dryout and mist zones. For flow patterns such as intermittent and annular the behavior of the heat transfer coefficient shows an increasing trend; at the beginning of the dryout zone the HTC tends to decrease for increasing vapor quality [8]. The working fluid reaches a quasi-total caloric balance with the pipe, and when reaching the mist zone, it completely changes its phase from liquid to vapor, and thus the HTC in the dryout and mist zones tends to decrease to minimum values of 516.37 $W\cdot m^{-2}\cdot K^{-1}$ for the example shown.
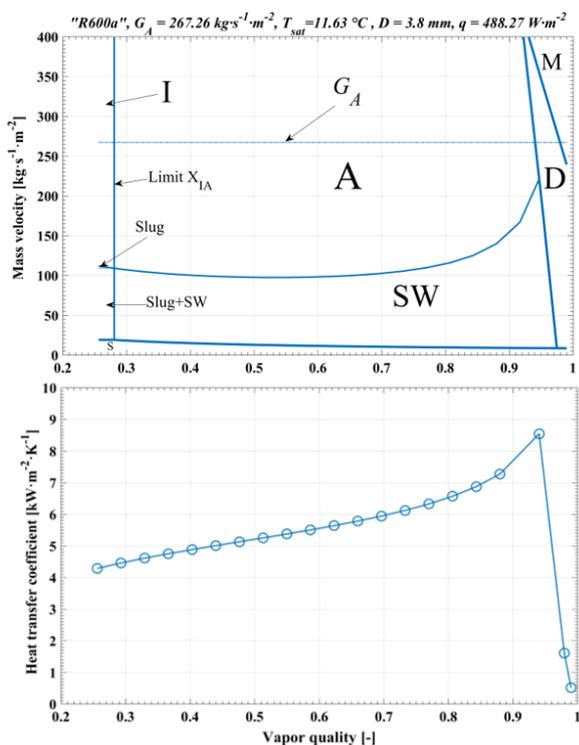

Figure 13. Contrasting of flow pattern maps vs. heat transfer coefficient for the Wojtan *et al.* [8], [28] mathematical model

4. Conclusions

The flow pattern maps obtained in the experimental tests conducted represent the behavior of the phase change of the R600a refrigerant, in response to the solar energy gained by the system. The plots and the limits of the different flow regimes showed a variation based on the different operating parameters, namely: mass velocity, incident solar radiation, heat flux, mass flow [23] and initial quality of the working fluid. Similarly, the flow pattern maps enable studying the different configurations of the distribution of two phases in a fluid, and indicate which zone predicts its almost total phase change; for that purpose, the following conclusions were obtained:

The predominant zones in this study are intermittent, annular and dryout, since these are the flows present in all tests, and the dryout and mist zones present in different opportunities. This is the case of the mist zone, which will be present when the heat flux and the mass velocity are 488.27 $W\cdot m^{-2}$ and 267.26 $kg\cdot m^{-2}\cdot s^{-1}$, respectively, whereas for the stratified-wavy zone the heat flux and the mass velocity will be 72.83 $W\cdot m^{-2}$ and 197.59 $kg\cdot m^{-2}\cdot s^{-1}$, respectively.

The stratified-wavy zone was present in tests D and E, at quality ranges 0.952-0.961 and 0.939-0.968, respectively. Whereas, the mist zone is present in test B with quality range 0.979-0.99 and in test C with quality range 0.982-0.99. In addition, tests D and E were obtained with incident solar radiation values of 123.22 and 0 $W\cdot m^{-2}$, respectively.

Since test A has an initial quality of 0.176, it is more similar to the model of flow pattern map considered as base for this study. However, in tests B and C it is visualized the largest dryout and mist zones, thus fulfilling the condition that the fluid must enter the compressor in vapor phase.

The present research work was conducted using an environmentally friendly refrigerant, such as R600a isobutane, which has an ODP of 0 and a GWP of 3; moreover, its use presents larger thermal conductivities compared to conventional refrigerants such as R22 and R134a.

Acknowledgements

References

[1] J. Calle-Sigüencia and O. Tinoco-Gómez, "Obtención de ACS con energía solar en el cantón Cuenca y análisis de la contaminación ambiental," *Ingenius*, no. 19, pp. 89–101, 2018. [Online]. Available: https://doi.org/10.17163/ings.n19.2018.09

[2] W. Quitiaquez, J. Estupiñán Campos, C. Isaza Roldán, F. Toapanta-Ramos, and A. Lobato-Campoverde, "Análisis numérico de

Quitiaquez et al. / Numerical analysis of flow pattern map of R600a in a collector/evaporator of a solar-assisted heat pump

119

un sistema de calentamiento de agua utilizando un colector solar de placa plana," *Ingenius*, no. 24, pp. 97–106, 2020. [Online]. Available: https://doi.org/10.17163/ings.n24.2020.10

[3] N. Abas, A. R. Kalair, N. Khan, A. Haider, Z. Saleem, and M. S. Saleem, "Natural and synthetic refrigerants, global warming: A review," *Renewable and Sustainable Energy Reviews*, vol. 90, pp. 557–569, 2018. [Online]. Available: https://doi.org/10.1016/j.rser.2018.03.099

[4] K. Nawaz, B. Shen, A. Elatar, V. Baxter, and O. Abdelaziz, "R290 (propane) and R600a (isobutane) as natural refrigerants for residential heat pump water heaters," *Applied Thermal Engineering*, vol. 127, pp. 870–883, 2017. [Online]. Available: https://doi.org/10.1016/j.applthermaleng.2017.08.080

[5] C.-C. Yu and T.-P. Teng, "Retrofit assessment of refrigerator using hydrocarbon refrigerants," *Applied Thermal Engineering*, vol. 66, no. 1, pp. 507–518, 2014. [Online]. Available: https://doi.org/10.1016/j.applthermaleng.2014.02.050

[6] X. Zhuang, M. Gong, X. Zou, G. Chen, and J. Wu, "Experimental investigation on flow condensation heat transfer and pressure drop of R170 in a horizontal tube," *International Journal of Refrigeration*, vol. 66, pp. 105–120, 2016. [Online]. Available: https://doi.org/10.1016/j.ijrefrig.2016.02.010

[7] J. C. Pérez Angulo, C. Simancas, and N. Santos Santos, "Modelamiento y simulación de un sistema no convencional de levantamiento multifasico," *Fuentes, el reventón energético*, vol. 14, no. 1, pp. 19–34, 2016. [Online]. Available: https://doi.org/10.18273/revfue.v14n1-2016002

[8] L. Wojtan, T. Ursenbacher, and J. R. Thome, "Investigation of flow boiling in horizontal tubes: Part I–A new diabatic two-phase flow pattern map," *International Journal of Heat and Mass Transfer*, vol. 48, no. 14, pp. 2955–2969, 2005. [Online]. Available: https://doi.org/10.1016/j.ijheatmasstransfer.2004.12.012

[9] N. Kattan, J. R. Thome, and D. Favrat, "Flow boiling in horizontal tubes: Part 1–Development of a diabatic two-phase flow pattern map," *Journal of Heat Transfer*, vol. 120, no. 1, pp. 140–147, Oct. 1998. [Online]. Available: https://doi.org/10.1115/1.2830037

[10] H. Mashouf, M. Shafaee, A. Sarmadian, and S. Mohseni, "Visual study of flow patterns during evaporation and condensation of R-600a inside horizontal smooth and helically dimpled tubes," *Applied Thermal Engineering*, vol. 124, pp. 1392–1400, 2017. [Online]. Available: https://doi.org/10.1016/j.applthermaleng.2017.06.125

[11] A. Vahabi, M. Shafaee, A. Sarmadian, and H. Mashoof, "Discovering an empirically new relation and obtain the flow pattern map for dimpled tubes in two-phase flow for refrigerant R600-a," *Modares Mechanical Engineering*, vol. 17, no. 7, 2017. [Online]. Available: http://dorl.net/dor/20.1001.1.10275940.1396.17.7.25.7

[12] J. D. de Oliveira, J. B. Copetti, and J. C. Passos, "Experimental investigation on flow boiling pressure drop of R-290 and R-600a in a horizontal small tube," *International Journal of Refrigeration*, vol. 84, pp. 165–180, 2017. [Online]. Available: https://doi.org/10.1016/j.ijrefrig.2017.08.004

[13] Z.-Q. Yang, M. Gong, G. Chen, Z. Lin, H. Huang, and H. Feng, "A new diabatic two phase flow pattern transition model of R600a," *International Journal of Refrigeration*, vol. 99, pp. 138–144, 2019. [Online]. Available: https://doi.org/10.1016/j.ijrefrig.2018.12.025

[14] Y. Zhu, X. Wu, and R. Zhao, "R32 flow boiling in horizontal mini channels: Part I. Two-phase flow patterns," *International Journal of Heat and Mass Transfer*, vol. 115, pp. 1223–1232, 2017. [Online]. Available: https://doi.org/10.1016/j.ijheatmasstransfer.2017.07.101

[15] X. Zhuang, M. Gong, G. Chen, X. Zou, and J. Shen, "Two-phase flow pattern map for R170 in a horizontal smooth tube," *International Journal of Heat and Mass Transfer*, vol. 102, pp. 1141–1149, 2016. [Online]. Available: https://doi.org/10.1016/j.ijheatmasstransfer.2016.06.094

[16] J. Liu, J. Liu, and X. Xu, "Diabatic visualization study of R245fa two phase flow pattern characteristics in horizontal smooth and microfin tube," *International Journal of Heat and Mass Transfer*, vol. 152, p. 119513, 2020. [Online]. Available: https://doi.org/10.1016/j.ijheatmasstransfer.2020.119513

[17] J. Diehl de Oliveira, J. Biancon Copetti, and J. C. Passos, "An experimental investigation on flow boiling heat transfer of R-600a in a horizontal small tube," *International Journal of Refrigeration*, vol. 72, pp. 97–110, 2016. [Online]. Available: https://doi.org/10.1016/j.ijrefrig.2016.08.001

[18] M. Nasr, M. Akhavan-Behabadi, M. Momenifar, and P. Hanafizadeh, "Heat transfer characteristic of r-600a during flow boiling inside horizontal plain tube," *International Communications in Heat and Mass Transfer*, vol. 66, pp. 93–99, 2015. [Online]. Available: https://doi.org/10.1016/j.icheatmasstransfer.2015.05.024

[19] Z. Wang, P. Guo, H. Zhang, W. Yang, and S. Mei, "Comprehensive review on the development of sahp for domestic hot water," *Renewable and Sustainable Energy Reviews*, vol. 72, pp. 871–881, 2017. [Online]. Available: https://doi.org/10.1016/j.rser.2017.01.127

[20] D. Zhang, Q. Wu, J. Li, and X. Kong, "Effects of refrigerant charge and structural parameters on the performance of a direct-expansion solar-assisted heat pump system," *Applied Thermal Engineering*, vol. 73, no. 1, pp. 522–528, 2014. [Online]. Available: https://doi.org/10.1016/j.applthermaleng.2014.07.077

[21] G.-H. Shi, L. Aye, D. Li, and X.-J. Du, "Recent advances in direct expansion solar assisted heat pump systems: A review," *Renewable and Sustainable Energy Reviews*, vol. 109, pp. 349–366, 2019. [Online]. Available: https://doi.org/10.1016/j.rser.2019.04.044

[22] X. Kong, P. Sun, Y. Li, K. Jiang, and S. Dong, "Experimental studies of a variable capacity direct-expansion solar-assisted heat pump water heater in autumn and winter conditions," *Solar Energy*, vol. 170, pp. 352–357, 2018. [Online]. Available: https://doi.org/10.1016/j.solener.2018.05.081

[23] W. Quitiaquez, I. Simbaña, R. Caizatoa, C. Isaza, C. Nieto, P. Quitiaquez, and F. Toapanta, "Análisis del rendimiento termodinámico de una bomba de calor asistida por energía solar utilizando un condensador con recirculación," *Revista Técnica Energía*, vol. 16, no. 2, pp. 111–125, 2020. [Online]. Available: https://doi.org/10.37116/revistaenergia.v16.n2.2020.358

[24] G. K. Singh, S. Pradhan, and V. Tanna, "Experimental studies of two phase flow characteristics and void fraction predictions in steady state horizontal two-phase nitrogen flow," *Cryogenics*, vol. 100, pp. 77–84, 2019. [Online]. Available: https://doi.org/10.1016/j.cryogenics.2019.04.007

[25] C.-M. Yang and P. Hrnjak, "A new flow pattern map for flow boiling of R410a in horizontal micro-fin tubes considering the effect of the helix angle," *International Journal of Refrigeration*, vol. 109, pp. 154–160, 2020. [Online]. Available: https://doi.org/10.1016/j.ijrefrig.2019.09.013

[26] M. Shafaee, H. Mashouf, A. Sarmadian, and S. Mohseni, "Evaporation heat transfer and pressure drop characteristics of R-600a in horizontal smooth and helically dimpled tubes," *Applied Thermal Engineering*, vol. 107, pp. 28–36, 2016. [Online]. Available: https://doi.org/10.1016/j.applthermaleng.2016.06.148

[27] Z.-Q. Yang, G.-F. Chen, X.-R. Zhuang, Q.-L. Song, Z. Deng, J. Shen, and M.-Q. Gong, "A new flow pattern map for flow boiling of R1234ze(E) in a horizontal tube," *International Journal of Multiphase Flow*, vol. 98, pp. 24–35, 2018. [Online]. Available: https://doi.org/10.1016/j.ijmultiphaseflow.2017.08.015

[28] L. Wojtan, T. Ursenbacher, and J. R. Thome, "Investigation of flow boiling in horizontal tubes: Part II–Development of a new heat transfer model for stratified-wavy, dryout and mist flow regimes," *International Journal of Heat and Mass Transfer*, vol. 48, no. 14, pp. 2970–2985, 2005. [Online]. Available: https://doi.org/10.1016/j.ijheatmasstransfer.2004.12.013

[29] J. D. de Oliveira, J. C. Passos, J. B. Copetti, and C. van der Geld, "Flow boiling heat transfer of propane in 1.0 mm tube," *Experimental Thermal and Fluid Science*, vol. 96, pp. 243–256, 2018. [Online]. Available: https://doi.org/10.1016/j.expthermflusci.2018.03.010